GiVE: Guiding Visual Encoder to Perceive Overlooked Information

Junjie Li¹, Jianghong Ma¹, Xiaofeng Zhang*¹, Yuhang Li¹, Jianyang Shi¹

¹School of Computer Science and Technology, Harbin Institute of Technology, Shenzhen 22b351018@stu.hit.edu.cn, majianghong@hit.edu.cn, zhangxiaofeng@hit.edu.cn

Abstract

Multimodal Large Language Models have advanced AI in applications like text-to-video generation and visual question answering. These models rely on visual encoders to convert non-text data into vectors, but current encoders either lack semantic alignment or overlook non-salient objects. We propose the Guiding Visual Encoder to Perceive Overlooked Information (GiVE) approach. GiVE enhances visual representation with an Attention-Guided Adapter (AG-Adapter) module and an Object-focused Visual Semantic Learning module. These incorporate three novel loss terms: Objectfocused Image-Text Contrast (OITC) loss, Object-focused Image-Image Contrast (OIIC) loss, and Object-focused Image Discrimination (OID) loss, improving object consideration, retrieval accuracy, and comprehensiveness. Our contributions include dynamic visual focus adjustment, novel loss functions to enhance object retrieval, and the Multi-Object Instruction (MOInst) dataset. Experiments show our approach achieves state-of-the-art performance.

Introduction

The multimodal large language models (MLLMs) (Zhu et al. 2023; Liu et al. 2023b; Ye et al. 2023; Li et al. 2023) have significantly advanced general artificial intelligence by demonstrating exceptional capabilities in generation and inference across diverse real-world applications, such as textto-video generation (Blattmann et al. 2023), visual question answering (Singh et al. 2019), and embodied robotics (Mu et al. 2023). To optimize performance while managing costs, a prevalent MLLM architecture integrates a visual encoder with the large language model (LLM). This architecture encoder embeds non-text data, transforming these embeddings into vectors comprehensible to the LLM through a mapping mechanism. Although prior research (Wang et al. 2023; Liu et al. 2023a) has underscored the efficacy of this architecture, the cross-modal perception abilities of MLLMs heavily relies on the visual encoder, with the quality of encoded image embeddings directly influencing the response quality of the MLLMs.

An image encoder is a specialized visual encoder designed to map high-dimensional image data to a lower-dimensional feature space. These encoders can be broadly categorized based on their pre-training tasks into two main

types: reconstruction-based and cross-modal contrastive learning-based encoders.

- Image encoding models trained with reconstruction tasks (van den Oord, Vinyals, and Kavukcuoglu 2017; Huang, Fu, and Bors 2023) are proficient in capturing comprehensive image details. However, these models lack semantic alignment with text during training, which complicates the LLM's ability to interpret image embeddings (Yin et al. 2023). Consequently, such encoders are infrequently utilized in MLLMs.
- Vision transformer (ViT) models trained with imagetext contrastive learning (Radford et al. 2021; Jia et al. 2021) generally align effectively with LLMs but face an implicit "ignore" problem, limiting their expressive capability. This limitation arises because different modalities convey distinct types of information. For instance, an image may feature multiple objects with unique attributes, such as texture, color, spatial location, and potential interactions. In contrast, abstract text typically highlights only the most salient objects and provides limited descriptions of other visual elements. ViTs trained for image-text matching tend to focus on the salient regions of the image that correspond to the text, thereby overlooking secondary elements like the background. As shown in Table 13 of the Appendix, MLLMs using such visual encoders exhibit diminished response quality when users inquire about non-salient objects.

In summary, for effective integration with LLMs, MLLMs require an image encoder that is both (1) semantically aligned with text during training and (2) capable of flexible attention to prevent the omission of relevant visual features.

To address these challenges, we propose this Guiding Visual Encoder to Perceive Overlooked Information (GiVE) approach, which aims to guide the visual encoder in adaptively adjusting its attention to well capture overlooked information. In this approach, we introduce a novel Attention-Guided Adapter (AG-Adapter) module that enhances the representation ability of the visual encoder by aligning the visual representations with abstract semantics. This module also functions as a plug-in for generalizing abstract semantics, enabling it to more effectively address user queries.

To tackle the above limitations in detail, GiVE incorporates another innovative module: **Object-focused Visual**

^{*}Corresponding author.

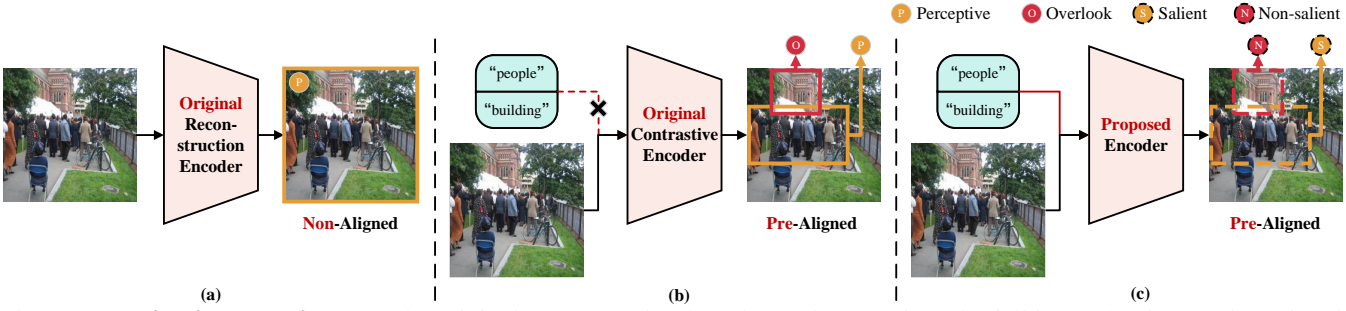


Figure 1: **Motivation overview**. (a) The original reconstruction-based encoder perceives the full image but is *not aligned with textual semantics*, thereby limiting its utility for LLMs in effectively interpreting the image embeddings. (b) The contrastive learning-based encoder only processes images *without the benefit of textual instructions*, leading to a focus *solely on salient objects* (P) and neglecting user-specific concerns (O). (c) Our proposed visual encoder addresses these limitations by flexibly adjusting its focus to highlight various objects, whether *salient* (S) or *non-salient* (N), according to the provided instructions.

Semantic Learning. This module employs three distinct model loss terms: (i) an Object-focused Image-Text Contrast (OITC) loss, which encourages the model to generate distinct embeddings for varied instructions, ensuring consideration of both salient and non-salient objects; (ii) an Object-focused Image-Image Contrast (OIIC) loss, which improves the accuracy of object retrieval by enabling the model to learn common features among in-class objects, thus enhancing concept generalization ability; and (iii) an Object-focused Image Discrimination (OID) loss, which improves the comprehensiveness of object retrieval by facilitating the model in identifying specific objects and recognizing potential correlations among objects, thereby preventing the omission of objects. As illustrated in Figure 1, GiVE enables visual encoders to generate image embeddings that are rich in targeted information.

Our contributions can be summarized as follows:

- We propose an innovative GiVE approach to give attetion to overlooked information, enabling dynamic adjustment of focus by modifying textual instructions. This capability allows for flexible and adaptive attention to various objects within the image.
- We propose three novel loss functions: OITC, OIIC, and OID. The OITC loss addresses the current limitations of the original visual encoder, particularly its neglect of non-salient objects. The OIIC loss enhances ungeneralized representation ability, thereby improving object retrieval accuracy. The OID loss recognizes potential correlations among objects, further increasing the comprehensiveness of object retrieval.
- We present a fine-grained image-text dataset with instructional labels, named the Multi-Object Instruction (MOInst) dataset, designed to provide semantic indications for different objects. Extensive experiments conducted on both constructed and real-world datasets showcase the effectiveness of our approach, achieving stateof-the-art performance.

Related Work

Pre-training Visual Encoders

Visual encoding models can be categorized based on their pre-training tasks into image reconstruction models and image-text contrast models. (i) Image reconstruction models, such as MAE (He et al. 2022), DeepMIM (Ren et al. 2023), and MIRL (Huang, Fu, and Bors 2023), use masked image modeling similar to language modeling. Other models, like VQ-VAE (van den Oord, Vinyals, and Kavukcuoglu 2017), VQGAN (Esser, Rombach, and Ommer 2021), and HQ-VAE (You et al. 2022), implement image reconstruction using autoencoder architectures. (ii) Models like CLIP (Radford et al. 2021), ALIGN (Jia et al. 2021), and EVA-CLIP (Sun et al. 2023) utilize cross-modal contrastive learning to align textual and visual information into a unified semantic space. Consequently, such pre-aligned encoders are more readily aligned with LLMs through alignment pre-training (Yin et al. 2023). In contrast, reconstruction-trained models lack this text correlation due to their independent training process. As detailed in Table 5 in the Appendix, 90% of the MLLMs we investigated use image-text contrast encoders.

Discussion. Our study preserves the semantic alignment capabilities of visual encoders while minimizing the omission of effective information by using semantic instructions.

Visual Perception of MLLMs

Despite some pioneering works mitigating the negative effects of visual ignorance, they still have limitations. For instance, InstructBLIP (Dai et al. 2023) injects textual instructions to guide the post-processing process with a lightweight Q-Former to translate the image embeddings. However, this downstream secondary coding only reinforces indicationrelated information in the image embeddings and does not recover useful features lost in the upstream image encoder. Similarly, LLaVA-NeXT (Liu et al. 2024) encodes the image multiple times after segmentation, allowing each subimage to have its own salient object, thus reducing the visual feature loss rate. However, this exponentially increases token occupancy and encoding time. Additionally, BLIVA (Hu et al. 2024) combines the mapper of BLIP-2 and LLaVA to enhance the LLM's understanding from more translation perspectives, but since both mappers share the same image encoder, this method does not fundamentally address the loss of useful information during visual encoding.

Dicussion. Overlooking the inherent imperfections of visual encoders and attempting to rectify them through alternative means is frequently inadequate. Our objective is to

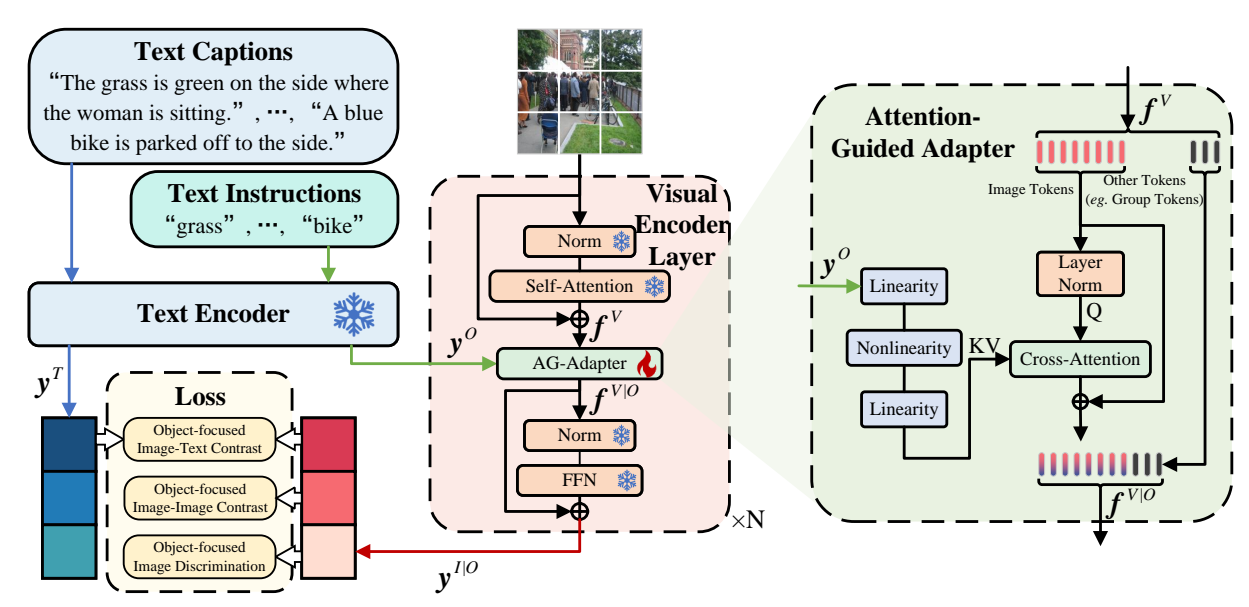


Figure 2: **Overall architecture of GiVE**. The plug-in module, AG-Adapter, is inserted into the feature extraction layers of the visual encoder and trained with the three losses proposed in our work: Object-focused Image-Text Contrast (OITC), Object-focused Image-Image Contrast (OIIC), and Object-focused Image Discrimination (OID). Cross-attention is used to emphasize the visual elements most relevant to the textual instructions. The text instructions are pre-integrated into the prompt template designated as "a photo of {object}".

confront these shortcomings directly within the visual encoder, thereby minimizing the accumulation of errors from the outset of the encoding process.

Methodology

The proposed approach takes a text encoder to encode both captions and instructions, and a visual encoder for visual content. An AG-Adapter module is inserted into each stacked visual encoder as the tunable parameters to align cross-modal data. The AG-Adapter is trained by the designed Object-focused Visual Semantic Learning module. Details of model architecture, AG-Adapter, and object-focused visual semantic learning module are presented in the following subsections. The overall architecture is depicted in Figure 2.

Model Architecture

The proposed model includes a visual encoder $\Phi_I(\cdot,\cdot)$ and a text encoder $\Phi_T(\cdot)$ to respectively encode visual and textual content. It accepts image-text-object triplets $\{\boldsymbol{x}^I, \boldsymbol{x}^T, \boldsymbol{x}^O\}$ as input, where $\boldsymbol{x}^I \in \mathcal{I}$ is an image, $\boldsymbol{x}^T \in \mathcal{T}$ is a text, and $\boldsymbol{x}^O \in \mathcal{O}$ is an indicative text denoting the target object, such as "person". The model then extracts conditional image and text features $(\boldsymbol{y}^{I|O}, \boldsymbol{y}^T)$ using paired encoders. When extracting conditional image features, the instruction feature \boldsymbol{y}^O is fused with the visual data stream within the AG-Adapter module. Formally,

$$y^{T} = \Phi_{T}(x^{T}), \ y^{O} = \Phi_{T}(x^{O}), \ y^{I|O} = \Phi_{I}(x^{I}, y^{O}),$$
(1)

where $\boldsymbol{y}^T \in \mathbb{R}^d$ is text feature, $\boldsymbol{y}^O \in \mathbb{R}^d$ is instruction feature, and $\boldsymbol{y}^{I|O}$ is conditional image feature, i.e. the output of the visual encoder integrated with the AG-Adapter. The AG-Adapter is trained using our designed Object-focused Visual Semantic Learning component containing three loss terms:

OITC, OIIC and OID. Note that during the training phase, the loss is calculated based on the output embeddings of both encoders. During the inference phase, the text encoder is retained to serialize the textual instructions.

Attention-guided Adapter

The proposed AG-Adapter module, as highlighted in green rectangle in Figure 2, is a simple yet effective plug-in that interweaves semantic directives with visual cues, enabling visual model to perceive queried objects. The AG-Adapter is inspired by Latent Diffusion Model (LDM) (Rombach et al. 2022) which enhances the alignment of visual representations with abstract semantics by conditioning on text representations. In particular, the AG-Adapter is incorporated into the pre-training feature extraction layers of the $\Phi_I(\cdot,\cdot)$, with only the inserted layer undergoing the training process.

Formally, in each layer of the visual encoder, the AG-Adapter module $\varphi(\cdot)$ enhances fine-grained object features:

$$\boldsymbol{f}^{V|O} = \varphi(\boldsymbol{y}^O, \boldsymbol{f}^V), \tag{2}$$

where \boldsymbol{y}^O is instruction feature derived from user queries and \boldsymbol{f}^V refers to the feature of the visual data flow. The $\boldsymbol{f}^V \in \mathbb{R}^{(M+K)\times d}$ is composed of two types of tokens: image tokens $\boldsymbol{f}^I \in \mathbb{R}^{M\times d}$ and other tokens $\boldsymbol{f}^H \in \mathbb{R}^{K\times d}$. The image tokens are derived directly from the input image, while the role of other tokens depends on the baseline model. In the case of GroupViT (Xu et al. 2022), other tokens are group tokens; in contrast, in CLIP (Radford et al. 2021), they are absent, and K=0. Within the AG-Adapter, the dual-layer MLP serves to bridge the gap between text and image representations, namely,

$$\boldsymbol{f}^{O} = MLP(\boldsymbol{y}^{O}), \tag{3}$$

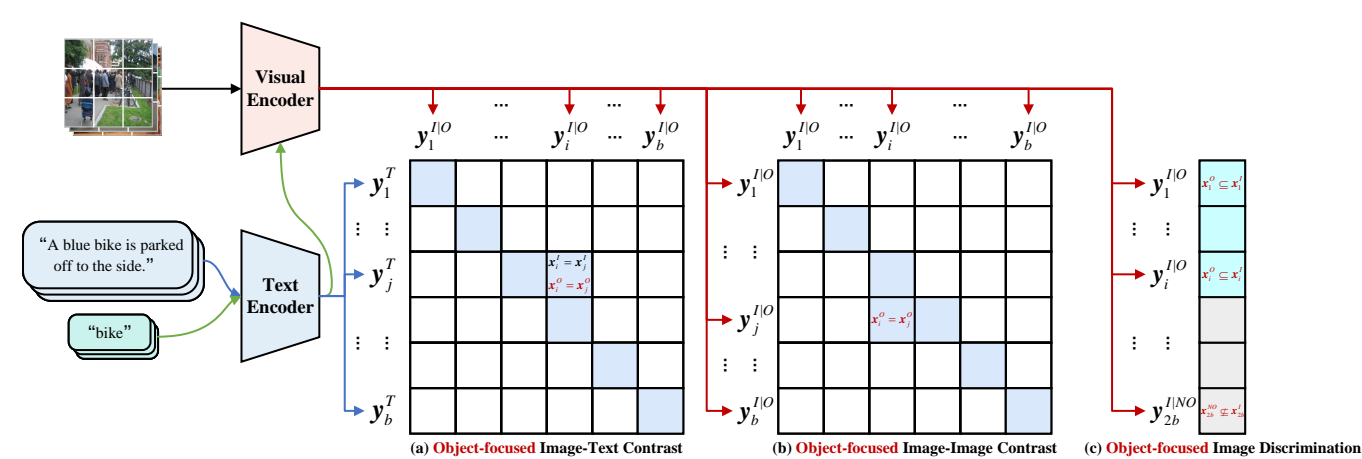


Figure 3: Learning objectives illustration. The image and text encoders jointly compute three losses. (a) For Object-focused Image-Text Contrast, the paired text and image should not only correspond to each other but also correspond to the same semantic object. (b) Object-focused Image-Image Contrast requires the model to predict pairs of image features that contain the same semantic object. (c) Object-focused Image Discrimination determines whether a specific object exists or not in the image. The text instructions, such as "bike", are pre-integrated into the prompt template designated as "a photo of {object}".

where $MLP(\cdot)$ denotes two linear mappings and one nonlinear mapping. The image tokens are standardized in order to enhance training stability:

$$\hat{\boldsymbol{f}}^I = \text{Norm}(\boldsymbol{f}^I), \tag{4}$$

 $\hat{\pmb{f}}^I = \text{Norm}(\pmb{f}^I),$ (4) where Norm(·) denotes the layer normalization operater. Subsequently, $oldsymbol{f}^O$ and $\hat{oldsymbol{f}}^I$ are merged through the crossattention mechanism, with the resulting fused features integrated back into the visual data stream through residual concatenation as

$$\mathbf{f}^{I|O} = \mathbf{f}^{I} + \operatorname{Cross}(\hat{\mathbf{f}}^{I}, \mathbf{f}^{O}), \tag{5}$$

where $\mathrm{Cross}(\cdot,\cdot)$ represents a cross-attention operator, $\hat{\boldsymbol{f}}^I$ is treated as query and \boldsymbol{f}^O is key and value. $\boldsymbol{f}^{I|O}$ emphasizes the semantic objects while maintaining the integrity of the original visual information. The resulting tokens are then concatenated with other tokens to form the final features:

$$\boldsymbol{f}^{V|O} = [\boldsymbol{f}^{I|O}; \boldsymbol{f}^H], \tag{6}$$

where [;] represents the concatenation of two vectors. The feature $f^{V|O}$ that enriches the visual information of the indicated object is fed to the subsequent module.

In this module, we counter-intuitively use the image as the query and the text as the key and value. This approach is driven by two considerations. First, it ensures that visual information is adequately preserved. Typically, instruction tokens are much shorter than image tokens, so a text-based query might not carry sufficient information. Second, the LDM (Rombach et al. 2022) conditions the image feature delivery on the text, also using the image as the query and the text as the key and value, indicating that such modal fusion is feasible. Our subsequent experiments confirm the effectiveness of this role assignment.

Object-focused Visual Semantic Learning

During the abstract concept learning phase, the original parameters of the image and text encoders are frozen, and the parameters of the AG-Adapter are trained. In each training batch, we sample b image-text-object triples $\{\boldsymbol{x}_k^I, \boldsymbol{x}_k^T, \boldsymbol{x}_k^O\}_{k=1}^b$ and encode them to obtain image-text feature pairs $\{\boldsymbol{y}_k^{I|O}, \boldsymbol{y}_k^T\}_{k=1}^b$. Our goal is to train the AGAdapter to extract the most relevant visual representations based on semantic instructions. As shown in Figure 3, to achieve this goal, we jointly optimize three training objectives that share model parameters.

Object-focused Image-Text Contrast (OITC) objective is designed to align image and text representations centered around instructed objects, with the aim of maximizing their mutual information. This objective requires the visual encoder to generate distinct features for different instructions. The similarity between features is computed as follows:

$$s_{i,i}^{I|O} = s_{i,i}^{T} = (\mathbf{y}_{i}^{I|O})^{\top} \mathbf{y}_{i}^{T},$$
 (7)

 $s_{i,j}^{I|O} = s_{i,j}^T = (\boldsymbol{y}_i^{I|O})^\top \boldsymbol{y}_j^T, \tag{7}$ where $s_{i,j}^{I|O}$ denotes the similarity of the *i*-th conditional image feature to the *j*-th text feature, and $s_{i,j}^T$ represents the similarity between the *i*-th text feature and the *j*-th text feature. For the conditional image feature $oldsymbol{y}_k^{I|O}$ in feature pair $\{\boldsymbol{y}_k^{I|O}, \boldsymbol{y}_k^T\}$, the corresponding text features $m{y}_{j|m{x}_j^I=m{x}_k^I\wedgem{x}_j^O=m{x}_k^O}^T$ of the same object within the same image are positive, while other text features within the batch are negative. The loss of a batch can be represented by

$$\mathcal{L}_{k}^{I|O}(\boldsymbol{y}_{k}^{I|O}, \{\boldsymbol{y}_{j}^{T}\}_{j=1}^{b}) = -\frac{1}{b}\log\frac{\sum_{k,j}\exp(s_{k,j}^{I|O}\mid\boldsymbol{x}_{j}^{I}=\boldsymbol{x}_{k}^{I}\wedge\boldsymbol{x}_{j}^{O}=\boldsymbol{x}_{k}^{O})}{\sum_{j}\exp(s_{k,j}^{I|O})}, \quad (8)$$

$$\mathcal{L}_{k}^{T}(\boldsymbol{y}_{k}^{T}, \{\boldsymbol{y}_{j}^{I|O}\}_{j=1}^{b}) = -\frac{1}{b}\log\frac{\sum_{k,j}\exp(s_{k,j}^{T}\mid\boldsymbol{x}_{j}^{I}=\boldsymbol{x}_{k}^{I}\wedge\boldsymbol{x}_{j}^{O}=\boldsymbol{x}_{k}^{O})}{\sum_{j}\exp(s_{k,j}^{T})}, \quad (9)$$

$$\mathcal{L}^{\text{OITC}} = \frac{1}{2} \sum_{k=1}^{b} (\mathcal{L}_k^{I|O} + \mathcal{L}_k^T), \tag{10}$$

where $\mathcal{L}_k^{I|O}$ is image-to-text contrastive loss, \mathcal{L}_k^T is text-to-image contrastive loss, and $\mathcal{L}^{\text{OITC}}$ is total loss.

Object-focused Image-Image Contrast (OIIC) loss emphasizes the commonality of objects within the same class, requiring the encoder to generate similar features for these objects. The contrast is performed within the image. For a feature $\boldsymbol{y}_k^{I|O}$, $\boldsymbol{y}_j^{I|O}_{|\boldsymbol{x}_j^O|=\boldsymbol{x}_k^O}$ is its positive example, while other conditional image features in the batch serve as in-batch negatives. The similarity computation of conditional image features is expressed as

$$s_{i,j} = (\boldsymbol{y}_i^{I|O})^\top \boldsymbol{y}_j^{I|O}. \tag{11}$$

The OIIC loss, denoted by \mathcal{L}^{OIIC} , can be represented as

$$\mathcal{L}^{\text{OIIC}} = -\frac{1}{b} \sum_{k=1}^{b} \log \frac{\sum_{k,j} \exp(s_{k,j} \mid \boldsymbol{x}_{j}^{O} = \boldsymbol{x}_{k}^{O})}{\sum_{j} \exp(s_{k,j})}.$$
 (12)

Model	LVI	\mathbb{S}^f	LVI	\mathbb{S}^a
Model	F1	AUC	F1	AUC
Instruct.	-0.1	49.9	0.1	50.0
CLIP-ViT	11.3	57.8	8.6	55.5
+ GiVE	50.7	75.6	56.2	77.3
Improv.	348.7%	30.8%	553.5%	39.3%
$GroupViT_y$	9.6	56.8	7.3	54.8
+ GiVE	31.9	65.3	42.3	69.8
Improv.	232.3%	15.0%	479.5%	27.4%
$GroupViT_r$	10.1	57.2	8.2	55.4
+ GiVE	31.8	65.9	42.8	70.3
Improv.	214.9%	15.2%	422.0%	26.9%
SigLIP	10.7	57.3	9.0	55.6
+ GiVE	48.6	74.2	53.0	75.0
Improv.	354.2%	29.5%	488.9%	34.9%
OwlViT	0.0	50.0	0.0	50.0
+ GiVE	40.6	70.6	41.8	69.9
Improv.	-	41.2%	-	39.8%

Table 1: Top-1 F1 and AUC (%) of zero-shot image classification on multi-object datasets. "Instruct." signifies that classification is based on the instruction text rather than the image. "GroupViT $_y$ " and "GroupViT $_r$ ", i.e., GroupViTgcc-yfcc and GroupViT-gcc-redcaps, denote two variants of GroupViT trained with different datasets, respectively. Since our evaluation metric accounts for and subtracts the influence of textual interference, it can result in negative values.

Object-focused Image Discrimination (OID) is a binary classification task that requires the model to predict whether a given image and the indicated object match. For each batch of sample pairs $\{\boldsymbol{x}_k^I, \boldsymbol{x}_k^O\}_{k=1}^b$, we additionally construct b negative pairs $\{\boldsymbol{x}_k^I, \boldsymbol{x}_k^{NO}\}_{k=1}^b$, where \boldsymbol{x}_k^{NO} indicating object not appear in \boldsymbol{x}_k^I . These positive and negative samples $\{\boldsymbol{x}_k^I, \boldsymbol{x}_k^{O\cup NO}\}_{k=1}^{2b}$ are encoded to $\{\boldsymbol{y}_k^{I|O\cup NO}\}_{k=1}^{2b}$, which are then input into a binary linear classifier to obtain

Model	# TP		\rightarrow Text	Text →	_
		R@1	R@5	R@1	R@5
Instruct.		0.1	0.1	-0.2	0.4
CLIP-ViT	88M	7.6	18.7	5.4	19.7
+ GiVE	62M	29.1	53.3	29.8	54.9
Improv.		282.9%	185.0%	451.9%	178.7%
$GroupViT_y$	31M	5.9	18.0	4.2	17.8
+ GiVE	15M	13.2	29.3	16.7	34.9
Improv.		123.7%	62.8%	297.6%	96.1%
$GroupViT_r$	31M	7.2	19.1	4.7	18.7
+ GiVE	15M	12.6	29.8	17.1	36.2
Improv.		75.0%	56.0%	263.8%	93.6%
SigLIP	93M	9.3	23.6	6.9	25.6
+ GiVE	85M	20.7	43.6	25.7	48.1
Improv.		122.6%	84.7%	272.5%	87.9%
OwlViT	88M	5.6	16.5	4.1	16.5
+ GiVE	62M	12.4	32.1	14.4	35.2
Improv.		121.4%	94.5%	251.2%	113.3%

Table 2: Fine-tuned image-text retrieval results on MOInst dataset. "# TP" denotes the number of trainable parameters.

logits $\{z_k\}_{k=1}^{2b}$. The loss function is formalized as

$$p_i = \frac{1}{1 + \exp(-z_i)},\tag{13}$$

$$\mathcal{L}^{\text{OID}} = -\frac{1}{2b} \sum_{i=1}^{2b} [t_i \log(p_i) + (1 - t_i) \log(1 - p_i)], \quad (14)$$

where $p_i \in \mathbb{R}$ and $t_i \in \{0, 1\}$ denote the predicted probability and true label of the *i*-th sample, respectively.

Please refer to Appendix Figure 5 and the accompanying introduction for the inference pipeline.

Instruction of New Dataset

Although the Visual Genome (VG) dataset (Krishna et al. 2017) provides multiple objects and captions per image, it lacks object-caption correspondence, features noisy labels, and contains low-quality text. Therefore, it is not recommended to use the VG dataset directly. To address these issues, we construct the Multi-Object Instruction (MOInst) dataset. This dataset comprises 81,536 high-fidelity, complex images, accompanied by 244,378 textual captions. Each caption is associated with one of 264 distinct categories. Additional details are available in the Appendix.

Experiments

Experimental Setup

Datasets We evaluate the effectiveness of GiVE using both the LVIS dataset (Gupta, Dollár, and Girshick 2019) and MOInst dataset, each annotating multiple objects per image. The comprehensive LVIS dataset, referred to as LVIS a , comprises 1,203 categories, from which, we derive a subset, denoted as LVIS f , with 405 "frequent" categories. In contrast, the MOInst dataset used for training contains 264 categories, with category label overlaps of 7.7% and 17.6% with the two LVIS datasets, respectively. We also conduct

							MC	Inst	LVI	\mathbb{S}^f	LVI	\mathbb{S}^a
Model	# TP	Inst.	Img Enc.	Type	GiVE	Post Proc.	I2T R@1	T2I R@1	F1	AUC	F1	AUC
BLIP-2	1.2B	X	EVA-CLIP-ViT	G/14	X	Q-Former	14.1	9.4	14.1	58.2	11.3	56.3
BLIP-2	388M	/	CLIP-ViT	B/32	/	Q-Former	30.1	31.1	35.2	67.4	40.1	68.9
Improv.							113.5%	230.9%	149.6%	15.8%	254.9%	22.4%
InstructBLIP	1.2B	/	EVA-CLIP-ViT	G/14	X	Q-Former	19.8	22.1	28.6	64.7	23.0	60.9
InstructBLIP	388M	/	CLIP-ViT	B/32	/	Q-Former	24.2	21.9	35.0	67.1	42.7	70.6
Improv.							22.2%	-0.9%	22.4%	3.7%	85.7%	15.9%
AG-CLIP	62M	/	CLIP-ViT	B/32	/	_	29.1	29.8	50.7	75.6	56.2	77.3

Table 3: The effect of semantic instructions on secondary coding methods. AG-CLIP is CLIP-ViT with GiVE for attention guidance. "Inst." indicates whether the model receives additional instructions. "Img Enc." specifies the image encoder used by the model, and "Type" denotes the type of image encoder. "GiVE" shows whether our GiVE method is applied to the image encoder, and "Post Proc." identifies the type of post-processor used for the secondary encoding of the image embeddings.

experiments on the COCO (Lin et al. 2014), SUN397 (Xiao et al. 2010), and ImageNet (Gao et al. 2023) datasets.

Baselines We evaluate the gains brought by integrating the GiVE with several representative ViT baselines, including CLIP (Radford et al. 2021), GroupViT (Xu et al. 2022), SigLIP (Zhai et al. 2023), and OwlViT (Minderer et al. 2022). GroupViT has two versions trained on different datasets, and OwlViT is a visual encoder designed for object detection. Additionally, we apply the GiVE to BLIP-2 (Li et al. 2023) and InstructBLIP (Dai et al. 2023) to explore its impact within a larger encoding framework. Throughout this paper, unless explicitly stated otherwise, the experiments with GiVE are conducted on the CLIP platform, with the unmarked CLIP model referring to CLIP-ViT-B/32. Furthermore, a comparison is presented between CLIP using GiVE and the more recent MetaCLIP (Xu et al. 2024).

Evaluation Metrics Inspired by prior works (Li et al. 2023; Yao et al. 2022), we conduct quantitative evaluations on image classification and image-text retrieval tasks. Scores are calculated solely from vector similarity, without further optimization, to accurately reflect the effective information content of the extracted features. To ensure that the scores reflect the visual information extraction capabilities of visual encoders, we mitigate the potential interference by quantifying the influence of textual data when evaluating methods that use instruction text, such as InstructBLIP (Dai et al. 2023). For detailed calculations and implementation specifics, see the Appendix.

Performance Evaluation

Image Classification We conduct zero-shot image classification on the "frequent" subset and the full LVIS test set. Table 1 presents the results on five ViT baselines. Key observations from these experiments are as follows:

- The evaluation value for the instruction text is nearly equivalent to random categorization, demonstrating that our metric successfully filters out textual interference. This outcome ensures that our work fairly compares the visual feature extraction capabilities of each model.
- The GiVE demonstrates a notable improvement in all baselines across all metrics on both evaluation datasets.

			MO	Inst	LV	IS^f	LV	IS^a
Loss	Fuse	Inst.	I2T R@1	T2I R@1	F1	AUC	F1	AUC
X	X	X	7.6	5.4	11.3	57.8	8.6	55.5
-OITC	early+late	✓	0.1	0.1	0.3	50.0	0.1	50.0
-OIIC	early+late	/	28.1	29.4	48.4	74.0	55.7	76.7
-OID	early+late	/	28.1	29.7	37.6	67.8	47.6	72.2
all	early	✓	6.4	8.2	27.7	63.6	37.2	67.3
all	late	/	27.1	29.1	47.4	73.6	55.6	76.5
all	sparse	/	27.0	29.0	46.9	73.0	55.1	76.3
all	early+late	X	0.0	0.1	0.3	50.0	0.4	50.0
all	early+late (dense)	/	29.1	29.8	50.7	75.6	56.2	77.3

Table 4: Ablation study. The "fuse" represents the layer where the AG-Adapter is inserted. The "early" indicates feature fusion in only the first half of the layers near the input, while the "late" indicates fusion in the latter half. The "sparse" refers to fusion in alternating layers, whereas the "dense" means fusion in all layers.

This highlights the efficacy of the GiVE's capacity to redirect attention based on semantic instructions.

- OwlViT, a ViT designed for object detection, requires fine-tuning to serve effectively as an image feature extractor. However, GiVE can unlock its potential.
- The AG-Adapter, trained on the MOInst dataset with 264 classes, achieves F1 scores of over 40% on the LVIS^a dataset with 1,203 classes. The observed gaps in category magnitudes indicate that the instruction semantics have generalizability beyond the training scope.

Please see Table 11 in the Appendix for a comparison with MetaCLIP on more datasets.

Image-Text Retrieval Image-text retrieval includes two subtasks: image-to-text retrieval and text-to-image retrieval. We evaluate the models on the MOInst dataset. Since the AG-Adapter is trained on this dataset, we compare the results under the fine-tuned setting, as recorded in Table 2.

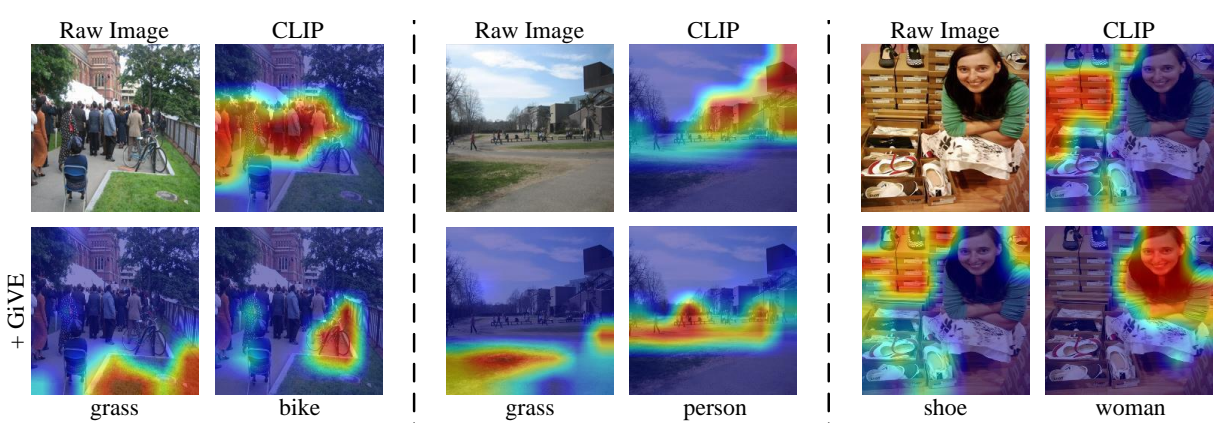


Figure 4: **Visual encoder attention visualization**. The images are divided into three groups, each containing the raw image and its attention visualization. The first row shows the raw image and the attention of CLIP-ViT. The second row displays attention maps of CLIP integrated with the AG-Adapter under various instructions.

As shown in Table 2, GiVE outperforms all baseline methods while utilizing fewer trainable parameters. And the informativeness gap between instruction and caption, illustrated in Figure 5 of Appendix, indicates that simple instruction alone is insufficient for the model to achieve such a high hit rate. Together, GiVE effectively extracts target visual features. Additionally, the evaluation results for "Instruct." further support the credibility of our experimental findings.

Comparison with Secondary Coding Methods The BLIP-2 and InstructBLIP methods utilize a Q-Former to re-encode image features after the visual encoder, with InstructBLIP incorporating text instructions into the Q-Former. We replace the visual encoders of these two methods with AG-CLIP-ViT-B/32 and then fine-tune them on MOInst following their respective strategies. The results are shown in Table 3. From the table, it can be observed that:

- Our AG-CLIP shows performance improvements compared to the original BLIP-2 and InstructBLIP, despite the significant difference in the number of parameters. This supports the validity of injecting instructions.
- Semantic instructions prove to be more efficient during visual feature extraction than when applied post-process. In our second set of experiments, we replace the original giant EVA-CLIP in InstructBLIP with the base AG-CLIP, resulting in superior performance across most metrics. Although AG-CLIP performs slightly worse in the textto-image retrieval task, the substantial difference in the number of training parameters makes this acceptable.
- Secondary encoding may weaken the abstract semantics in the visual features, leading to decreased performance in image classification tasks, as evidenced by the superior performance of AG-CLIP compared to BLIP-2 and InstructBLIP on LVIS^f and LVIS^a datasets.

Ablation Studies

In this section, we conduct an ablation study of the GiVE from three perspectives: loss, fusion layers, and abstract semantic instructions. Specifically, for instructions, we eliminate abstract semantics by replacing short object prompts with detailed descriptions. Table 4 presents the experimental results, with the gray row representing the original CLIP-

ViT and the yellow row representing our AG-CLIP-ViT. Observations from the results are as follows:

- The ablation study on loss functions suggests that all three losses are crucial, with particular emphasis on the OITC loss, which is responsible for aligning objectfocused visual features with text features.
- The late encoding layers have a significantly greater impact on abstract semantics compared to the early and sparse layers, though the early and sparse layers also contribute to the understanding of semantics.
- In the absence of instructions, captions can serve as textual inputs. However, overly specific captions may cause the visual encoder to rely heavily on textual instructions, possibly missing key details in the image.

Attention Visualization

In this section, we use EigenCAM (Muhammad and Yeasin 2020) to visualize the attention of CLIP-ViT with and without the integration of the GiVE on three example images in Figure 4. It is evident that GiVE aids the original ViT in encoding images more effectively in the following ways:

- Flexibility for a single image. The dynamically changing attention areas in each image indicate that the ViT no longer encodes fixed image features but can extract visual features tailored to the query.
- Effectiveness of semantic control over attention. The three attention distributions for the left and middle images show that even objects initially overlooked by the ViT can be brought into focus through instructions.
- Completeness of object retrieval. As shown in the right image with the "shoe" instruction, all shoes are attended to, regardless of whether they are in a box or separated by a human body. GiVE enables the ViT to locate more comprehensive specific objects.

For additional results, see Figure 7 in the Appendix.

Conclusion

This paper presents GiVE, a novel approach enhancing visual encoders' integration with LLMs by addressing semantic alignment and overlooked information. GiVE features

the AG-Adapter and three innovative loss functions—OITC, OIIC, and OID. The AG-Adapter aligns visual representations with abstract semantics, while the OITC loss ensures attention to both salient and non-salient objects, and the OIIC and OID losses enhance object retrieval accuracy and comprehensiveness. Experiments show GiVE's significant improvements over existing methods in multiple tasks.

References

- Bai, J.; Bai, S.; Yang, S.; Wang, S.; Tan, S.; Wang, P.; Lin, J.; Zhou, C.; and Zhou, J. 2023. Qwen-VL: A Versatile Vision-Language Model for Understanding, Localization, Text Reading, and Beyond. *arXiv preprint arXiv:2308.12966*.
- Blattmann, A.; Rombach, R.; Ling, H.; Dockhorn, T.; Kim, S. W.; Fidler, S.; and Kreis, K. 2023. Align Your Latents: High-Resolution Video Synthesis with Latent Diffusion Models. In *IEEE/CVF Conference on Computer Vision and Pattern Recognition, CVPR 2023, Vancouver, BC, Canada, June 17-24*, 2023, 22563–22575. IEEE.
- Chen, J.; Zhu, D.; Shen, X.; Li, X.; Liu, Z.; Zhang, P.; Krishnamoorthi, R.; Chandra, V.; Xiong, Y.; and Elhoseiny, M. 2023a. MiniGPT-v2: large language model as a unified interface for vision-language multi-task learning. *CoRR*, abs/2310.09478.
- Chen, K.; Zhang, Z.; Zeng, W.; Zhang, R.; Zhu, F.; and Zhao, R. 2023b. Shikra: Unleashing Multimodal LLM's Referential Dialogue Magic. *arXiv preprint arXiv:2306.15195*.
- Chen, L.; Li, J.; Dong, X.; Zhang, P.; He, C.; Wang, J.; Zhao, F.; and Lin, D. 2023c. ShareGPT4V: Improving Large Multi-Modal Models with Better Captions. *arXiv preprint arXiv:2311.12793*.
- Chen, Y.; Sikka, K.; Cogswell, M.; Ji, H.; and Divakaran, A. 2023d. DRESS: Instructing Large Vision-Language Models to Align and Interact with Humans via Natural Language Feedback. *CoRR*, abs/2311.10081.
- Chen, Y.; Sikka, K.; Cogswell, M.; Ji, H.; and Divakaran, A. 2023e. Measuring and Improving Chain-of-Thought Reasoning in Vision-Language Models. *CoRR*, abs/2309.04461.
- Cherti, M.; Beaumont, R.; Wightman, R.; Wortsman, M.; Ilharco, G.; Gordon, C.; Schuhmann, C.; Schmidt, L.; and Jitsev, J. 2023. Reproducible Scaling Laws for Contrastive Language-Image Learning. In *IEEE/CVF Conference on Computer Vision and Pattern Recognition, CVPR* 2023, Vancouver, BC, Canada, June 17-24, 2023, 2818–2829. IEEE.
- Dai, W.; Li, J.; Li, D.; Tiong, A. M. H.; Zhao, J.; Wang, W.; Li, B.; Fung, P.; and Hoi, S. C. H. 2023. InstructBLIP: Towards General-purpose Vision-Language Models with Instruction Tuning. In *Advances in Neural Information Processing Systems 36: Annual Conference on Neural Information Processing Systems*.
- Esser, P.; Rombach, R.; and Ommer, B. 2021. Taming Transformers for High-Resolution Image Synthesis. In *CVPR*, 12873–12883. Computer Vision Foundation / IEEE.
- Gao, S.; Li, Z.; Yang, M.; Cheng, M.; Han, J.; and Torr, P. H. S. 2023. Large-Scale Unsupervised Semantic Segmenta-

- tion. IEEE Trans. Pattern Anal. Mach. Intell., 45(6): 7457–7476.
- Girdhar, R.; El-Nouby, A.; Liu, Z.; Singh, M.; Alwala, K. V.; Joulin, A.; and Misra, I. 2023. ImageBind One Embedding Space to Bind Them All. In *CVPR*, 15180–15190. IEEE.
- Gupta, A.; Dollár, P.; and Girshick, R. B. 2019. LVIS: A Dataset for Large Vocabulary Instance Segmentation. In *IEEE Conference on Computer Vision and Pattern Recognition*, 5356–5364.
- He, K.; Chen, X.; Xie, S.; Li, Y.; Dollár, P.; and Girshick, R. B. 2022. Masked Autoencoders Are Scalable Vision Learners. In *CVPR*, 15979–15988. IEEE.
- Hu, W.; Xu, Y.; Li, Y.; Li, W.; Chen, Z.; and Tu, Z. 2024. BLIVA: A Simple Multimodal LLM for Better Handling of Text-Rich Visual Questions. In *Thirty-Eighth AAAI Conference on Artificial Intelligence*, 2256–2264.
- Huang, G.; Fu, H.; and Bors, A. G. 2023. Masked Image Residual Learning for Scaling Deeper Vision Transformers. In *NeurIPS*.
- Jia, C.; Yang, Y.; Xia, Y.; Chen, Y.; Parekh, Z.; Pham, H.; Le, Q. V.; Sung, Y.; Li, Z.; and Duerig, T. 2021. Scaling Up Visual and Vision-Language Representation Learning With Noisy Text Supervision. In *ICML*, volume 139 of *Proceedings of Machine Learning Research*, 4904–4916. PMLR.
- Krishna, R.; Zhu, Y.; Groth, O.; Johnson, J.; Hata, K.; Kravitz, J.; Chen, S.; Kalantidis, Y.; Li, L.; Shamma, D. A.; Bernstein, M. S.; and Fei-Fei, L. 2017. Visual Genome: Connecting Language and Vision Using Crowdsourced Dense Image Annotations. *Int. J. Comput. Vis.*, 123(1): 32–73.
- Li, J.; Li, D.; Savarese, S.; and Hoi, S. C. H. 2023. BLIP-2: Bootstrapping Language-Image Pre-training with Frozen Image Encoders and Large Language Models. In *International Conference on Machine Learning, ICML*, 19730–19742.
- Li, Y.; Zhang, Y.; Wang, C.; Zhong, Z.; Chen, Y.; Chu, R.; Liu, S.; and Jia, J. 2024. Mini-Gemini: Mining the Potential of Multi-modality Vision Language Models. *CoRR*, abs/2403.18814.
- Lin, T.; Maire, M.; Belongie, S. J.; Hays, J.; Perona, P.; Ramanan, D.; Dollár, P.; and Zitnick, C. L. 2014. Microsoft COCO: Common Objects in Context. In Fleet, D. J.; Pajdla, T.; Schiele, B.; and Tuytelaars, T., eds., Computer Vision ECCV 2014 13th European Conference, Zurich, Switzerland, September 6-12, 2014, Proceedings, Part V, volume 8693 of Lecture Notes in Computer Science, 740–755. Springer.
- Liu, H.; Li, C.; Li, Y.; and Lee, Y. J. 2023a. Improved Baselines with Visual Instruction Tuning. *CoRR*, abs/2310.03744.
- Liu, H.; Li, C.; Li, Y.; Li, B.; Zhang, Y.; Shen, S.; and Lee, Y. J. 2024. LLaVA-NeXT: Improved reasoning, OCR, and world knowledge.
- Liu, H.; Li, C.; Wu, Q.; and Lee, Y. J. 2023b. Visual Instruction Tuning. In *Advances in Neural Information Processing Systems 36: Annual Conference on Neural Information Processing Systems*.

- Liu, H.; Yan, W.; and Abbeel, P. 2023. Language Quantized AutoEncoders: Towards Unsupervised Text-Image Alignment. In *NeurIPS*.
- Liu, Z.; Mao, H.; Wu, C.; Feichtenhofer, C.; Darrell, T.; and Xie, S. 2022. A ConvNet for the 2020s. In *CVPR*, 11966–11976. IEEE.
- Maaz, M.; Rasheed, H. A.; Khan, S. H.; and Khan, F. S. 2023. Video-ChatGPT: Towards Detailed Video Understanding via Large Vision and Language Models. *CoRR*, abs/2306.05424.
- Mikolov, T.; Chen, K.; Corrado, G.; and Dean, J. 2013. word2vec Tool for Efficient Estimation of Word Representations in Vector Space. Accessed: 2024-08-07.
- Minderer, M.; Gritsenko, A.; Stone, A.; Neumann, M.; Weissenborn, D.; Dosovitskiy, A.; Mahendran, A.; Arnab, A.; Dehghani, M.; Shen, Z.; Wang, X.; Zhai, X.; Kipf, T.; and Houlsby, N. 2022. Simple Open-Vocabulary Object Detection with Vision Transformers. *ECCV*.
- Mu, Y.; Zhang, Q.; Hu, M.; Wang, W.; Ding, M.; Jin, J.; Wang, B.; Dai, J.; Qiao, Y.; and Luo, P. 2023. EmbodiedGPT: Vision-Language Pre-Training via Embodied Chain of Thought. In Advances in Neural Information Processing Systems 36: Annual Conference on Neural Information Processing Systems.
- Muhammad, M. B.; and Yeasin, M. 2020. Eigen-CAM: Class Activation Map using Principal Components. In 2020 International Joint Conference on Neural Networks, IJCNN 2020, Glasgow, United Kingdom, July 19-24, 2020, 1–7. IEEE.
- OpenAI. 2023. ChatGPT: Optimizing Language Models for Dialogue. https://openai.com/blog/chatgpt. Accessed: 2023-12-21.
- Oquab, M.; Darcet, T.; Moutakanni, T.; Vo, H.; Szafraniec, M.; Khalidov, V.; Fernandez, P.; Haziza, D.; Massa, F.; El-Nouby, A.; Assran, M.; Ballas, N.; Galuba, W.; Howes, R.; Huang, P.; Li, S.; Misra, I.; Rabbat, M. G.; Sharma, V.; Synnaeve, G.; Xu, H.; Jégou, H.; Mairal, J.; Labatut, P.; Joulin, A.; and Bojanowski, P. 2023. DINOv2: Learning Robust Visual Features without Supervision. *CoRR*, abs/2304.07193.
- Panagopoulou, A.; Xue, L.; Yu, N.; Li, J.; Li, D.; Joty, S.; Xu, R.; Savarese, S.; Xiong, C.; and Niebles, J. C. 2023. X-InstructBLIP: A Framework for aligning X-Modal instruction-aware representations to LLMs and Emergent Cross-modal Reasoning. *CoRR*, abs/2311.18799.
- Peng, Z.; Dong, L.; Bao, H.; Ye, Q.; and Wei, F. 2022. BEiT v2: Masked Image Modeling with Vector-Quantized Visual Tokenizers. *CoRR*, abs/2208.06366.
- Radford, A.; Kim, J. W.; Hallacy, C.; Ramesh, A.; Goh, G.; Agarwal, S.; Sastry, G.; Askell, A.; Mishkin, P.; Clark, J.; Krueger, G.; and Sutskever, I. 2021. Learning Transferable Visual Models From Natural Language Supervision. In *Proceedings of the 38th International Conference on Machine Learning, ICML*, volume 139, 8748–8763.
- Ren, S.; Wei, F.; Albanie, S.; Zhang, Z.; and Hu, H. 2023. DeepMIM: Deep Supervision for Masked Image Modeling. *CoRR*, abs/2303.08817.

- Rombach, R.; Blattmann, A.; Lorenz, D.; Esser, P.; and Ommer, B. 2022. High-Resolution Image Synthesis with Latent Diffusion Models. In *IEEE/CVF Conference on Computer Vision and Pattern Recognition, CVPR*, 10674–10685. IEEE.
- Singh, A.; Natarajan, V.; Shah, M.; Jiang, Y.; Chen, X.; Batra, D.; Parikh, D.; and Rohrbach, M. 2019. Towards vqa models that can read. In *IEEE/CVF conference on computer vision and pattern recognition*, 8317—8326.
- Su, Y.; Lan, T.; Li, H.; Xu, J.; Wang, Y.; and Cai, D. 2023. PandaGPT: One Model To Instruction-Follow Them All. *arXiv preprint arXiv:2305.16355*.
- Sun, Q.; Fang, Y.; Wu, L.; Wang, X.; and Cao, Y. 2023. EVA-CLIP: Improved Training Techniques for CLIP at Scale. *CoRR*, abs/2303.15389.
- Tang, Z.; Yang, Z.; Khademi, M.; Liu, Y.; Zhu, C.; and Bansal, M. 2024. CoDi-2: In-Context Interleaved and Interactive Any-to-Any Generation. In *Proceedings of the IEEE/CVF Conference on Computer Vision and Pattern Recognition (CVPR)*, 27425–27434.
- THUDM. 2023. VisualGLM-6B. https://github.com/THUDM/VisualGLM-6B. GitHub repository.
- van den Oord, A.; Vinyals, O.; and Kavukcuoglu, K. 2017. Neural Discrete Representation Learning. In *NIPS*, 6306–6315.
- Wang, W.; Lv, Q.; Yu, W.; Hong, W.; Qi, J.; Wang, Y.; Ji, J.; Yang, Z.; Zhao, L.; Song, X.; Xu, J.; Xu, B.; Li, J.; Dong, Y.; Ding, M.; and Tang, J. 2023. CogVLM: Visual Expert for Pretrained Language Models. *CoRR*, abs/2311.03079.
- Wu, S.; Fei, H.; Qu, L.; Ji, W.; and Chua, T. 2023. NExT-GPT: Any-to-Any Multimodal LLM. *CoRR*, abs/2309.05519.
- Xiao, J.; Hays, J.; Ehinger, K. A.; Oliva, A.; and Torralba, A. 2010. SUN database: Large-scale scene recognition from abbey to zoo. In *CVPR*, 3485–3492. IEEE Computer Society.
- Xu, H.; Xie, S.; Tan, X. E.; Huang, P.; Howes, R.; Sharma, V.; Li, S.; Ghosh, G.; Zettlemoyer, L.; and Feichtenhofer, C. 2024. Demystifying CLIP Data. In *ICLR*. OpenReview.net. Xu, J.; Mello, S. D.; Liu, S.; Byeon, W.; Breuel, T. M.; Kautz, J.; and Wang, X. 2022. GroupViT: Semantic Segmentation Emerges from Text Supervision. In *IEEE/CVF Conference on Computer Vision and Pattern Recognition, CVPR*, 18113–18123. IEEE.
- Yang, Z.; Zhang, Y.; Meng, F.; and Zhou, J. 2023. TEAL: Tokenize and Embed ALL for Multi-modal Large Language Models. *CoRR*, abs/2311.04589.
- Yao, L.; Huang, R.; Hou, L.; Lu, G.; Niu, M.; Xu, H.; Liang, X.; Li, Z.; Jiang, X.; and Xu, C. 2022. FILIP: Fine-grained Interactive Language-Image Pre-Training. In *The Tenth International Conference on Learning Representations, ICLR*. OpenReview.net.
- Ye, Q.; Xu, H.; Xu, G.; Ye, J.; Yan, M.; Zhou, Y.; Wang, J.; Hu, A.; Shi, P.; Shi, Y.; Li, C.; Xu, Y.; Chen, H.; Tian, J.; Qi, Q.; Zhang, J.; and Huang, F. 2023. mPLUG-Owl: Modularization Empowers Large Language Models with Multimodality. *CoRR*, abs/2304.14178.

Ye, Q.; Xu, H.; Ye, J.; Yan, M.; Hu, A.; Liu, H.; Qian, Q.; Zhang, J.; and Huang, F. 2024. mPLUG-Owl2: Revolutionizing Multi-modal Large Language Model with Modality Collaboration. In *Proceedings of the IEEE/CVF Conference on Computer Vision and Pattern Recognition (CVPR)*, 13040–13051.

Yin, S.; Fu, C.; Zhao, S.; Li, K.; Sun, X.; Xu, T.; and Chen, E. 2023. A Survey on Multimodal Large Language Models. *CoRR*, abs/2306.13549.

You, T.; Kim, S.; Kim, C.; Lee, D.; and Han, B. 2022. Locally Hierarchical Auto-Regressive Modeling for Image Generation. In *NeurIPS*.

Yu, L.; Cheng, Y.; Wang, Z.; Kumar, V.; Macherey, W.; Huang, Y.; Ross, D. A.; Essa, I.; Bisk, Y.; Yang, M.; Murphy, K. P.; Hauptmann, A. G.; and Jiang, L. 2023. SPAE: Semantic Pyramid AutoEncoder for Multimodal Generation with Frozen LLMs. In *NeurIPS*.

Zhai, X.; Mustafa, B.; Kolesnikov, A.; and Beyer, L. 2023. Sigmoid Loss for Language Image Pre-Training. In *IEEE/CVF International Conference on Computer Vision, ICCV 2023, Paris, France, October 1-6, 2023*, 11941–11952. IEEE.

Zhang, H.; Li, X.; and Bing, L. 2023. Video-LLaMA: An Instruction-tuned Audio-Visual Language Model for Video Understanding. In *EMNLP (Demos)*, 543–553. Association for Computational Linguistics.

Zhao, H.; Zhang, M.; Zhao, W.; Ding, P.; Huang, S.; and Wang, D. 2024. Cobra: Extending Mamba to Multi-Modal Large Language Model for Efficient Inference. *CoRR*, abs/2403.14520.

Zhao, Y.; Lin, Z.; Zhou, D.; Huang, Z.; Feng, J.; and Kang, B. 2023. BuboGPT: Enabling Visual Grounding in Multi-Modal LLMs. *CoRR*, abs/2307.08581.

Zheng, K.; He, X.; and Wang, X. E. 2023. MiniGPT-5: Interleaved Vision-and-Language Generation via Generative Vokens. *CoRR*, abs/2310.02239.

Zhu, D.; Chen, J.; Shen, X.; Li, X.; and Elhoseiny, M. 2023. MiniGPT-4: Enhancing Vision-Language Understanding with Advanced Large Language Models. *CoRR*, abs/2304.10592.

Reproducibility Checklist

This paper:

- Includes a conceptual outline and/or pseudocode description of AI methods introduced (yes)
- Clearly delineates statements that are opinions, hypothesis, and speculation from objective facts and results (yes)
- Provides well marked pedagogical references for lessfamiliare readers to gain background necessary to replicate the paper (yes)

Does this paper make theoretical contributions? (no) Does this paper rely on one or more datasets? (yes)

A motivation is given for why the experiments are conducted on the selected datasets (yes)

- All novel datasets introduced in this paper are included in a data appendix. (yes)
- All novel datasets introduced in this paper will be made publicly available upon publication of the paper with a license that allows free usage for research purposes. (yes)
- All datasets drawn from the existing literature (potentially including authors' own previously published work) are accompanied by appropriate citations. (yes)
- All datasets drawn from the existing literature (potentially including authors' own previously published work) are publicly available. (yes)
- All datasets that are not publicly available are described in detail, with explanation why publicly available alternatives are not scientifically satisficing. (NA)

Does this paper include computational experiments? (yes)

- Any code required for pre-processing data is included in the appendix. (yes)
- All source code required for conducting and analyzing the experiments is included in a code appendix. (yes)
- All source code required for conducting and analyzing the experiments will be made publicly available upon publication of the paper with a license that allows free usage for research purposes. (yes)
- All source code implementing new methods have comments detailing the implementation, with references to the paper where each step comes from (yes)
- If an algorithm depends on randomness, then the method used for setting seeds is described in a way sufficient to allow replication of results. (NA)
- This paper specifies the computing infrastructure used for running experiments (hardware and software), including GPU/CPU models; amount of memory; operating system; names and versions of relevant software libraries and frameworks. (yes)
- This paper formally describes evaluation metrics used and explains the motivation for choosing these metrics. (yes)
- This paper states the number of algorithm runs used to compute each reported result. (yes)
- Analysis of experiments goes beyond single-dimensional summaries of performance (e.g., average; median) to include measures of variation, confidence, or other distributional information. (yes)
- The significance of any improvement or decrease in performance is judged using appropriate statistical tests (e.g., Wilcoxon signed-rank). (partial)
 - The methodology presented in this paper is demonstrably superior to existing baselines for our tasks, and its efficacy is not merely attributable to random fluctuations. Consequently, statistical testing is not a necessary component of this evaluation.
- This paper lists all final (hyper-)parameters used for each model/algorithm in the paper's experiments. (yes)



Appendix

The appendix covers several key topics: first, it provides an example of the inference pipeline to illustrate the GiVE workflow. Next, it presents statistics on the types of image encoders used by MLLMs. Following this, it describes the proposed MOInst dataset and its construction process. The appendix then details the experimental setup and includes additional experiments, such as parameter sensitivity and visualization illustrations. Finally, it demonstrates the impact of visual attention on MLLMs and the improvements achieved with our GiVE approach.

Prompt Engineering and Pipeline

GiVE aims to provide text guided visual coding scheme. Text is a medium that is readily comprehensible and straightforward for both humans and models. Therefore, we chose to utilize text, which introduces the challenge of avoiding information leakage. To mitigate this issue, we provide only minimal information to the visual encoder, specifically words that serve as object labels. This level of information is sufficient to prevent the visual encoder from missing key features.

However, text encoders are typically trained on complete sentences describing images rather than single words. To address this discrepancy, object indicator words are incorporated into the template "A photo of {object}" during both training and inference. Figure 5 illustrates the pipeline of the model as an example of image-text retrieval.

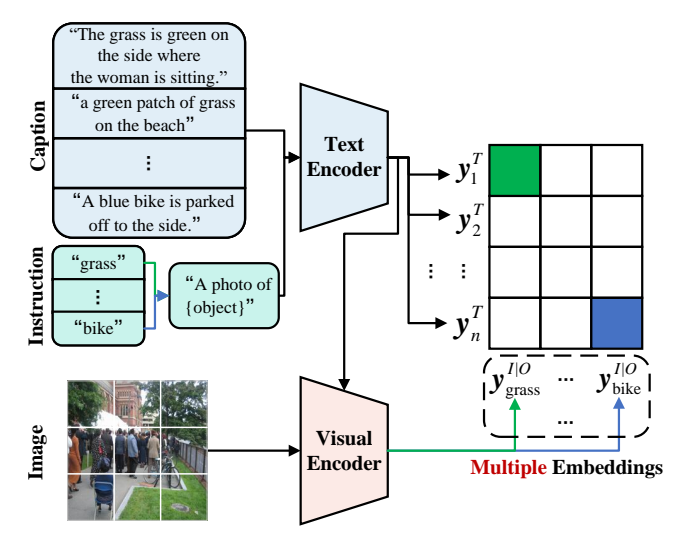


Figure 5: **Pipeline for image-text retrieval**. The frozen text encoder synthesizes retrieval instructions through constructed statements with target objects. The trained image encoder generates corresponding image embeddings for different instructions.

MLLM and Image Encoder Summary

An investigation was conducted into 30 common MLLMs from the past two years, with a view to establish which image encoders they employ and the pre-training tasks associ-

ated with these encoders. The findings are set out in Table 5. It is evident that the majority of researchers prefer prealigned encoders such as CLIP (Radford et al. 2021) when constructing MLLM models. Even the few models that employ image reconstruction encoders for specific purposes, such as expanding modalities (Yang et al. 2023) or freezing LLMs (Liu, Yan, and Abbeel 2023; Yu et al. 2023), exhibit diminished capacity for multimodal understanding in comparison to models like LLaVA (Liu et al. 2023b), whose encoders undergo training with contrastive learning.

Model	Image Encoder	Pre-training Task
BLIP-2 (2023)	CLIP (2021) /EVA-CLIP (2023)	contrast
InstructBLIP (2023)	CLIP (2021) /EVA-CLIP (2023)	contrast
X-InstructBLIP (2023)	EVA-CLIP (2023)	contrast
LLaVA (2023b)	CLIP (2021)	contrast
LLaVA-1.5 (2023a)	CLIP (2021)	contrast
LLaVA-NeXT (2024)	CLIP (2021)	contrast
BLIVA (2024)	EVA-CLIP (2023)	contrast
MiniGPT-4 (2023)	EVA-CLIP (2023)	contrast
MiniGPT-5 (2023)	EVA-CLIP (2023)	contrast
MiniGPT-v2 (2023a)	EVA-CLIP (2023)	contrast
mPLUG-Owl (2023)	CLIP (2021)	contrast
mPLUG-Owl2 (2024)	CLIP (2021)	contrast
ShareGPT4V (2023c)	CLIP (2021)	contrast
PandaGPT (2023)	ImageBind (2023)	contrast
Video-LLaMA (2023)	EVA-CLIP (2023)	contrast
Video-ChatGPT (2023)	CLIP (2021)	contrast
Shikra (2023b)	CLIP (2021)	contrast
VisualGLM-6B (2023)	EVA-CLIP (2023)	contrast
CogVLM (2023)	EVA-CLIP (2023)	contrast
Mini-Gemini (2024)	CLIP (2021); ConvNeXt (2022)	contrast
BuboGPT (2023)	CLIP (2021) /EVA-CLIP (2023)	contrast
ChatSpot (2023)	CLIP (2021)	contrast
Qwen-VL (2023)	OpenCLIP (2023)	contrast
NExT-GPT (2023)	ImageBind (2023)	contrast
DRESS (2023d)	EVA-CLIP (2023)	contrast
Cobra (2024)	SigLIP (2023); DINOv2 (2023)	contrast
CoDi-2 (2024)	ImageBind (2023)	contrast
LQAE (2023)	LQAE (2023)	reconstruction
SPAE (2023)	SPAE (2023)	reconstruction
TEAL (2023)	BEiT-V2 (2022)	reconstruction

Table 5: A summary of common MLLMs and the image encoders they use. This table presents the image encoder pretraining tasks. Most researchers prefer using pre-aligned encoders when building MLLM models.

Multi-Object Instruction Dataset

Our MOInst dataset is divided into training and testing sets, and the specific statistics are shown in Table 6. The annotation files of Multi-Object Instruction (MOInst) encompass

Parts	# Imgs	# Caps	# Cats	# Avg. Cats/Image
Train	80536	240183	264	2.4
Test	1000	4195	264	3.2

Table 6: Statistics of the MOInst dataset. Parts represents the different partitions of the dataset, # Imgs indicates the total number of images in each partition, # Caps refers to the total number of captions, # Cats denotes the total number of distinct categories, and # Avg. Cats/Image is the average number of categories labeled per image. Multiple captions of an image may share the same category label.

the following fields: "image_id" indicates the unique identifier of a particular image, "file_name" serves as the image file name, "image_path" specifies the path to the image file, "caption" provides a textual description of an object in the image, "category_id" corresponds to the category identifier of the caption, and "object_id" uniquely identifies a particular category within a specific image. The key information for an image in the dataset is shown in Table 7 as an example.

Construction We refer to the pipeline of (Chen et al. 2023e) to construct our dataset. As shown in Figure 6, the pipeline consists of two stages. The first stage aims at generating category labels for the objects described by captions, while the second stage improves the quality of the labels.

- 1. We filter the raw caption data from the VG dataset based on metrics such as length. Additionally, we devise an initial prompt that briefly describes the data the LLM (GPT (OpenAI 2023) is used in this paper) should generate with reference to the examples. This prompt, along with the necessary context (caption text), is then used to generate a small sample set. Next, we inspect the generated samples and modify the prompt accordingly. Through several iterations, the refined prompt effectively guides the LLM in generating caption labels. The final prompt is described in Listing 1.
- 2. Although the labeling data roughly meets expectations, it faces issues due to the limitations of existing LLMs. These issues include confusion between singular and plural forms, overly fine divisions of category labels, and insufficient samples within certain categories. Therefore, the labeled data requires further processing. Initially, we obtain noun lemmas through lemmatization and merge labels derived from the same word. Subsequently, the word2vec model (Mikolov et al. 2013) is employed to derive the word embeddings for the labels, which are then utilized to calculate the similarity between them. Then, manual rules are set, including a similarity threshold and a minimum number of samples within a category, to cluster and filter the labels. By iterating these rules based on the merged data, the final dataset is obtained.

Experimental Setup

We introduce a new task for which no prior experimental data exists. As a result, we need to evaluate all models, including baselines and our proposed method. However, due

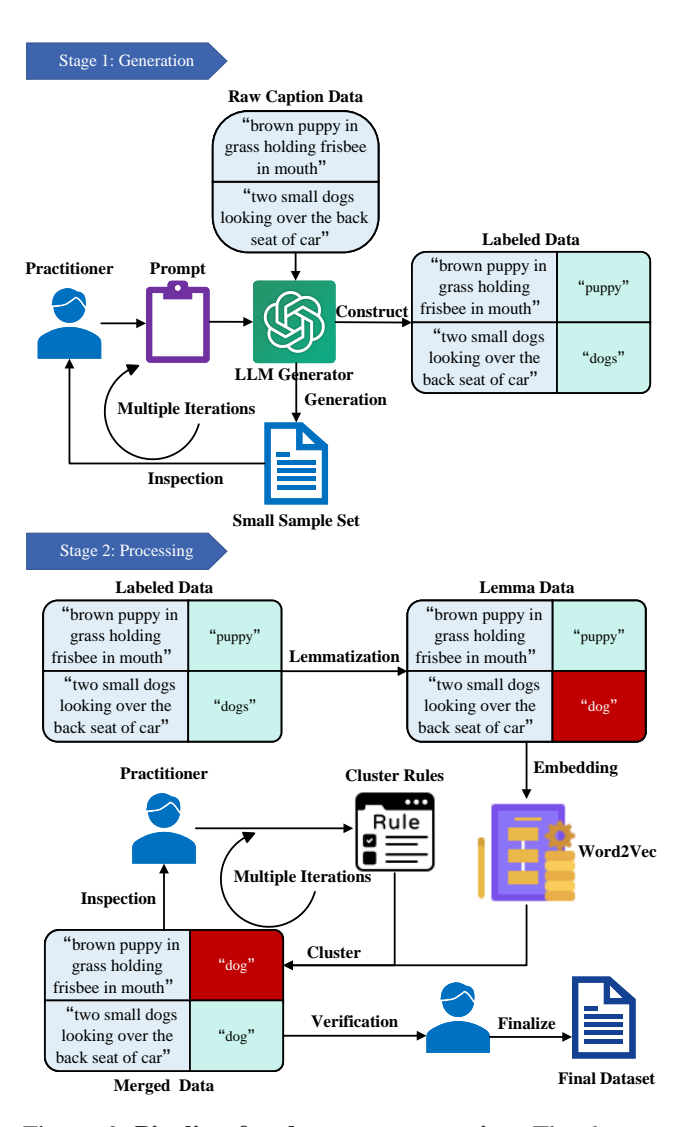


Figure 6: **Pipeline for dataset construction**. The dataset construction includes both generation and processing stages. It is created in a semi-automated manner with the help of existing models and minimal human assistance.

to limited computational resources, the cost of running multiple experiments to obtain error bars is prohibitively high. Consequently, it should be noted that the results presented in this paper are based on a single experiment.

Evaluation Metrics To obtain an accurate measure of visual encoding ability, it is essential to exclude the inflated values introduced by the instructional text. A way to quantify the impact of instructional information on the assessment is to calculate the probability that the results of task execution are consistent with an erroneous instruction. Specifically, for task $\tau(\cdot)$ and model $\Phi(\cdot, \cdot)$, a set of p evaluation data is given as $\{x_k^I, x_k^{IT}, t_k\}_{k=1}^p$, where x^{IT} represents the instruction text corresponding to the image x^I , and t is the ground truth. The evaluation score of the model can be for-

Image ID	Image	Category ID	Category	Object ID	Captions
484		2 31 36 130	fence bike woman grass	4840031	A fence made of metal by the road. A blue bike is parked off to the side. A woman is sitting down in a chair. The grass is green on the side where the woman is sitting.

Table 7: Important information about an image in the MOInst dataset. Image ID, Category ID, and Object ID are unique identifiers for images, category labels, and specific categories within a particular image, respectively.

```
Listing 1: The final prompt used in the MOInst construction
   You will label each sentence \mathbf{of} the
       given multiple sentences divided with
        <CAP>, the label indicates the
       object of the sentence. Labeling
       examples are given.
2
3
   labeling examples:
   a red car is at the back <CAP> two
       lights are on on the building <CAP>
       bikes are parked on the far end <CAP>
        the word \"walk\" is lit on a street
        sign <CAP> two men stand on an urban
        sidewalk
   car <LAB> light <LAB> bicycle <LAB>
       character <LAB> man
6
7
   sentences:
8
   {input_text}
9
   Indicate the subject of each sentence
       with prototype of one word separately
       , show me the labels directly without
        the sentences with each label
       separated by <LAB>, and make sure
       that the marked labels correspond one
```

malized as

$$S = \mathbb{E}[\mathbb{I}(\tau(\Phi(x_k^I, x_k^{IT})) = t_k)]. \tag{15}$$

Then the interference of the instruction text on the score can be expressed as

$$\mathcal{N} = \mathcal{S}(x_k^I, x_i^{IT}, t_i \mid j \neq k) \tag{16}$$

-to-one with the original sentence.

$$-S(x_k^I, x_i^{IT}, t_i \mid j \neq k, i \in \{1, 2, \dots, p\}), \quad (17)$$

which is the likelihood of being misdirected to a specific wrong minus randomness. Thus, the score obtained since the visual features are

$$S^V = S - \mathcal{N}. \tag{18}$$

Hyper-parameter Settings We report the hyper-parameter settings used during GiVE training in Table 8. All other settings align with those of the corresponding visual encoder.

Compute Resources We conduct our experiments on a NVIDIA A800-SXM4-80GB GPU, an Intel(R) Xeon(R) Platinum 8358P CPU @ 2.60GHz. The experimental device possesses 1.0 terabyte (TB) of memory, and its operating system is Ubuntu 22.04.3 LTS.

Item	Value	Item	Value
Optimizer Learning rate Epoch	5e-5	Batch size Weight decay Warmup ratio	

Table 8: Hyper-parameters for training the model.

				LV	$LVIS^f$ $LVIS$		IS^a
Type PS	# TP	I2T R@1	T2I R@1	F1	AUC	F1	AUC
B/32 32 ²	62M	29.1	29.8	50.7	75.6	56.2	77.3
B/16 16 ²							
$L/14 14^2$	240M	34.7	36.9	60.4	80.2	62.8	80.7

Table 9: Evaluation of the GiVE applied on different configurations of CLIP-ViT. "Type" refers to the type of the base model, "PS" indicates the patch size used when dividing the image into patches, and "# TP" represents the number of trainable parameters.

Parameter Sensitivity

Configurations of CLIP with GiVE We conduct experiments with different configurations of CLIP, and the results in Table 9 demonstrate that models integrated with the AG-Adapter can still be enhanced using typical methods. Specifically, smaller patch sizes can capture more fine-grained information, and an increased number of parameters can provide greater learning capacity. These enhancements improve CLIP's performance, and similarly, AG-CLIP, which combines CLIP with the GiVE, also benefits from these improvements.

Sensitivity Analysis on Loss Weights We also explore the impact of different loss weightings within GiVE on the AG-Adapter to balance the richness of effective information and the accuracy of semantic concepts. As observed from results in Table 10, variations in the weightings of these three hyperparameters cause the visual encoder's capabilities to favor one aspect of the trade-off over another. Taking everything into account, we adopt the relatively balanced values from the first row.

Comparison with Clip-based Method We compare CLIP (Radford et al. 2021), the recent MetaCLIP (Xu et al. 2024), and CLIP with our GiVE applied on five datasets for zero-shot image classification. The results, shown in Table

			MC	Inst	LV	IS^f	LV	IS^a
ω^{OITC}	$\omega^{ m OIIC}$	ω^{OID}	I2T R@1	T2I R@1	F1	AUC	F1	AUC
1	1	0.01	29.1	29.8	50.7	75.6	56.2	77.3
0.1	1	0.01	15.0	18.4	41.3	71.2	49.9	73.9
0.5	1	0.01	24.7	26.6	51.7	73.1	55.1	76.5
5	1	0.01	30.2	30.4	39.1	68.7	48.9	73.0
10	1	0.01	29.7	30.6	33.2	65.3	42.9	69.5
1	0.1	0.01	29.5	31.0	48.0	73.5	56.6	77.2
1	0.5	0.01	29.3	30.8	48.2	74.1	54.7	76.5
1	5	0.01	24.8	26.7	43.3	71.9	52.5	75.6
1	10	0.01	23.6	27.5	39.4	70.7	49.2	74.3
1	1	0.001	28.9	30.8	32.4	65.1	43.3	69.8
1	1	0.005	29.4	30.0	44.6	71.6	54.3	75.6
1	1	0.05	22.4	24.1	53.3	77.0	54.9	76.6
1	1	0.1	20.4	21.7	48.2	74.2	53.2	75.8

Table 10: Hyper-parameter grid search on $\omega^{\rm OITC}$, $\omega^{\rm OIIC}$, and $\omega^{\rm OID}$, which represent the weights for $\mathcal{L}^{\rm OITC}$, $\mathcal{L}^{\rm OIIC}$, and $\mathcal{L}^{\rm OID}$, respectively.

Model	LVIS ^f AUC	LVIS ^a AUC		SUN397 AUC	ImageNet AUC
CLIP	57.8	55.5	63.8	81.9	80.2
MetaCLIP	57.8	55.6	63.7	83.6	81.1
CLIP +GiVE	75.6	77.3	75.0	85.2	82.7

Table 11: Top-1 AUC (%) of zero-shot image classification on 5 datasets.

11, demonstrate that our method enables CLIP to outperform the state-of-the-art (SoTA) method.

Training Stability We apply our GiVE method to CLIP-ViT and repeat the experiment 5 times to calculate the mean and standard deviation, as recorded in Table 12. The results demonstrate that our method is relatively stable across all 3 tasks.

More Guided Attention Visualization

In Figure 7, we use EigenCAM (Muhammad and Yeasin 2020) to generate heat maps that visualize instruction following. The results demonstrate that our proposed method enables existing image encoder to flexibly perceive the query objects.

	MO	Inst	$LVIS^f$	$LVIS^a$
Model	I2T R@1	T2I R@1	AUC	AUC
CLIP +GiVE	29.1 ± 0.2	30.1 ± 0.3	75.3 ± 2.2	77.4 ± 1.1

Table 12: The means and standard deviations measured by CLIP with GiVE across 5 experiments on 3 different tasks.

Visual Attention and Response

Table 13 illustrates the disparate responses of MLLMs when queried with respect to disparate objects. The attention distributions of the visual encoders on images are visualized using EigenCAM (Muhammad and Yeasin 2020), with the redness intensity indicating the degree of attention the network allocates. The table presents a case study where the model accurately responds to a query about a highly salient SUV but incorrectly answers a query about a less noticeable car that shares features with the SUV. This error arises because the model's perception is constrained by image features that emphasize salient objects. When query information is incomplete, the model tends to default to common sense embedded in its weights. While this approach generally works for abstract text, it can lead to errors when dealing with detail-rich images.

In comparison, our GiVE aids in addressing the visual overlook issue. It enables the visual encoder to focus on the query object, even if it is non-salient. We substitute AG-CLIP-ViT-L/14, as referenced in Table 9, for CLIP-ViT-L/14, which is utilized by LLaVA (Liu et al. 2023b), without additional training. As illustrated in Table 14, this methodology allows LLaVA to generate a more accurate response.

Visual Input Example, Salience and Non-Salience Object Question:



Input image

LLaVA-1.5



CAM

User Describe in detail the SUV on the right.

LLaVA-1.5 Liu et al. 2023a) The SUV on the right is a yellow vehicle, possibly a van or a truck, with a man standing on the back of it. The man is holding a shirt, possibly ironing it or preparing to hang it on a clothesline. The SUV is parked on the side of the road, and it appears to be a unique and unconventional sight.

InstructBLIP (Dai et al. 2023) In the image, a yellow SUV is parked on the side of a busy city street. A man wearing a yellow shirt is standing on the back of the SUV, ironing clothes on an ironing board that is attached to the vehicle's roof rack. He is positioned in such a way that he can easily access the ironing board from the back of the SUV. The presence of the ironing board on top of the SUV adds a unique and creative touch to the scene, showcasing the man's resourcefulness and his ability to make the most out of his surroundings. Additionally, two taxis are visible in the background, adding to the bustling atmosphere of the city street.

User Describe in detail the car on the left.

LLaVA-1.5 (Liu et al. 2023a) The car on the left is a yellow taxi cab. It is driving down the street, and there is a man standing on the back of the car, holding a shirt. The taxi is passing by a building, and the man appears to be hanging the shirt on a clothesline.

InstructBLIP Dai et al. 2023) In the image, a man wearing a yellow shirt is seen standing on top of a car parked on the side of a busy city street. The car appears to be a large SUV or minivan, possibly a Toyota Highlander or Honda Odyssey. The man is ironing clothes on the roof of the vehicle, which is an unusual and creative way to do laundry in the middle of a bustling city. The presence of a yellow taxi cab nearby adds to the vibrant and lively atmosphere of the scene.

Table 13: Responses of MLLMs to queries on objects with varying attention levels.

Visual input example, Non-Salience Object Question:



User Describe in detail the car on the left.

LLaVA The car on the left is a yellow taxi cab. It is driving down the street, and a man is standing on the back of the car, holding a clothes iron. This unusual scene suggests that the man might be a tailor or a professional ironing service provider, offering his services to the people in the city.

LLaVA The car on the left is a yellow taxi cab. It is driving down the street, passing by a man who is
GiVE ironing clothes in the back of a truck. The taxi
cab is positioned behind the truck, and it appears to be in motion.

Table 14: The integration of GiVE enables MLLM to utilize more targeted visual features, thereby enhancing response quality. In the example, LLaVA with GiVE does not incorrectly position the man behind the car, and the response focuses on the car rather than mistakenly shifting emphasis to the man, as seen with the original LLaVA.

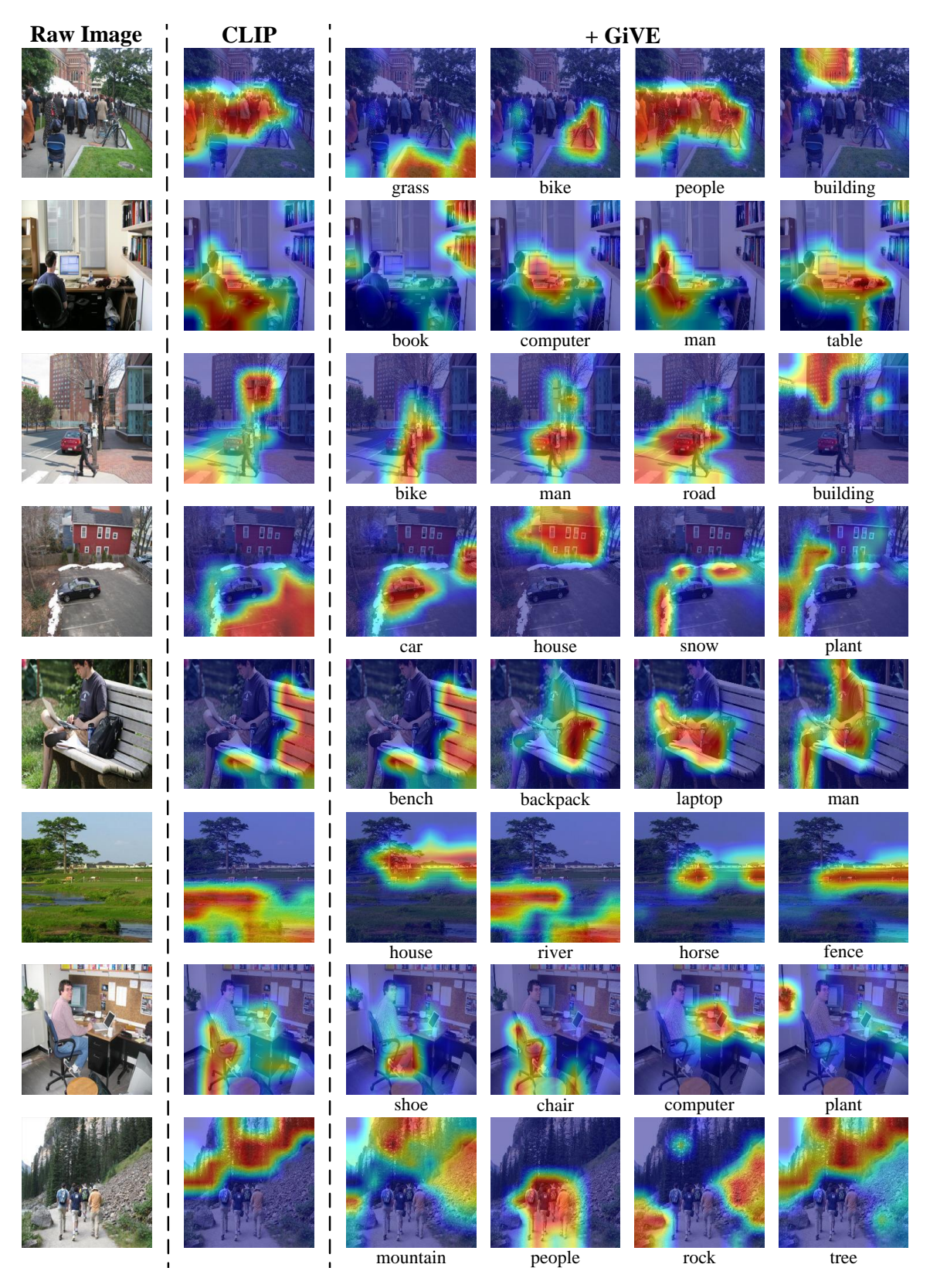


Figure 7: **More visualizations on different categories**. Each row represents a set, comprising the raw image and the visualized attention of the image encoders. The first column contains the raw image, the second column shows the attention of CLIP-ViT, and the last four columns illustrate how GiVE guides CLIP-ViT to attend to both salient and non-salient objects.